

Article

# Enhanced Photocatalytic Ozonation of Phenol by Ag/ZnO Nanocomposites

Junmin Peng<sup>1</sup>, Tong Lu<sup>1</sup>, Hongbo Ming<sup>1</sup>, Zhengxin Ding<sup>1</sup>, Zhiyang Yu<sup>1,2</sup>, Jinshui Zhang<sup>1</sup> and Yidong Hou<sup>1,\*</sup>

<sup>1</sup> State Key Laboratory of Photocatalysis on Energy and Environment, College of Chemistry, Fuzhou University, Fuzhou 350002, China; junminpeng@163.com (J.P.); tlutlutlu@163.com (T.L.); minghongbo@126.com (H.M.); zxding@fzu.edu.cn (Z.D.); yuzyemlab@gmail.com (Z.Y.); jinshui.zhang@fzu.edu.cn (J.Z.)

<sup>2</sup> Xiamen Tungsten Co., LTD. Xiamen 361126, China

\* Correspondence: ydhou@fzu.edu.cn; Tel.: +86-591-22865857

Received: 4 November 2019; Accepted: 27 November 2019; Published: 30 November 2019



**Abstract:** Ag/ZnO nanocomposites were synthesized and applied in the photocatalytic ozonation of phenol. Their crystal, textural, morphological, optical, and electrochemical properties were investigated by XRD, Raman, SEM, TEM, UV–Vis diffuse reflectance spectroscopy (DRS), X-ray photoemission spectroscopy (XPS), and photoluminescence (PL) techniques in detail. The results indicated that silver nanoparticles were well dispersed on the surface of porous ZnO and the intimate contacts were formed at the Ag/ZnO interfaces. This prominently favored the separation and transfer of photoinduced electrons from ZnO to Ag nanoparticles for the activation of ozone to produce  $\bullet\text{OH}$  and  $\bullet\text{O}_2^-$ . As a result, a significant enhancement in photocatalytic ozonation of phenol was achieved over Ag/ZnO catalysts. It also showed a synergistic effect between photocatalysis and ozonation.

**Keywords:** ZnO; silver; photocatalytic ozonation; phenol; synergistic effect

## 1. Introduction

The combination of ozone and heterogeneous photocatalysis is one of the promising advanced oxidation technologies for the decomposition of organic contaminants [1–3]. In this process, ozone can effectively capture the photogenerated electrons from the semiconductor to form ozonide radicals, which not only obviously inhibits the recombination of the electron-hole couples, but also remarkably increases the utilization efficiency of the dissolved ozone [4]. Thus, a significant enhancement in the decomposition and mineralization of organic pollutants should be realized in the process of photocatalytic ozonation. To advance the practical application of photocatalytic ozonation technology, it is highly desirable to develop high-performance catalysts that can initiate a great synergism in the combination of photocatalysis and ozonation [5–12].

As a typical semiconductor, ZnO is a promising candidate for photocatalytic ozonation reactions, owing to its good photocatalytic properties and unique function for ozonation activation [13–17]. In addition, easy synthesis, low cost, and environmental friendliness also enable the large-scale application of ZnO in the photocatalytic ozonation of organic pollutants [18]. However, owing to the rapid recombination of the photoexcited electron-hole pairs, the development of ZnO for photocatalytic ozonation reactions is greatly hindered and only moderate activity is achieved on pure ZnO for wastewater treatment [19].

Surface decoration of a semiconductor with metal nanoparticles is a facile and effective strategy to advance photocatalytic performances because the formation of heterostructure between metal and the semiconductor can greatly promote the separation and transfer of photogenerated electron-hole

pairs [20–23]. In addition, the supported metal nanoparticles can work with the semiconductor to cocatalyze chemical reactions [24–26]. In this study, Ag nanoparticles were employed to decorate ZnO for photocatalytic ozonation of organic pollutants by means of their unique properties. Experimentally, Ag nanoparticles were deposited onto the ZnO surface via a photochemical approach and the resultant Ag/ZnO catalysts were well investigated by XRD, Brunauer-Emmett-Teller (BET), TEM, SEM, X-ray photoemission spectroscopy (XPS), and electrochemical measurement. Phenol was chosen as a model contaminant to assess the catalytic performance. Electron paramagnetic resonance (EPR), along with quenching experiments, was conducted to probe the role of active species in the phenol removal and mineralization. Furthermore, the possible reaction mechanism over Ag/ZnO nanocomposites was proposed.

## 2. Results and Discussion

### 2.1. Catalysts Characterization

Figure 1a displays the XRD patterns of pure ZnO and Ag/ZnO samples. The strong and sharp diffraction peaks marked with “\*” can be assigned to the hexagonal wurtzite ZnO (JCPDS File No. 36-1451). The loading of Ag on ZnO does not change its crystal structure. When the Ag content increases to a certain amount (1.5 wt%) the characteristic diffraction peaks of Ag appear at 38.1° and 44.3° (JCPDS File No. 04-0783). The peak intensity becomes stronger with the increase of Ag content, indicating that the Ag/ZnO composite is successfully prepared. Furthermore, no shift in the ZnO diffraction peak is found among the samples, implying that Ag is deposited on the surface of ZnO rather than incorporated into the lattice of ZnO. Figure 1b presents the Raman spectra of ZnO and 1.5 wt% Ag/ZnO. The pure ZnO displays several bands at 433, 377, and 327  $\text{cm}^{-1}$ , corresponding to the  $E_2$ ,  $A_1(\text{TO})$ , and  $A_1$  modes of hexagonal wurtzite ZnO, respectively [27]. The strong  $E_2$  peak implies the good crystallinity of the ZnO nanoparticle. After loading the Ag nanoparticles, the intensity of the characteristic bands for ZnO is greatly increased, this is probably due to the local field of the metallic Ag on the surface of ZnO [28]. The new bands between 500 and 900  $\text{cm}^{-1}$  could originate from the enhanced Raman scattering by coupled LO-phonon-plasmon modes of ZnO with the presence of Ag nanoparticles [29].

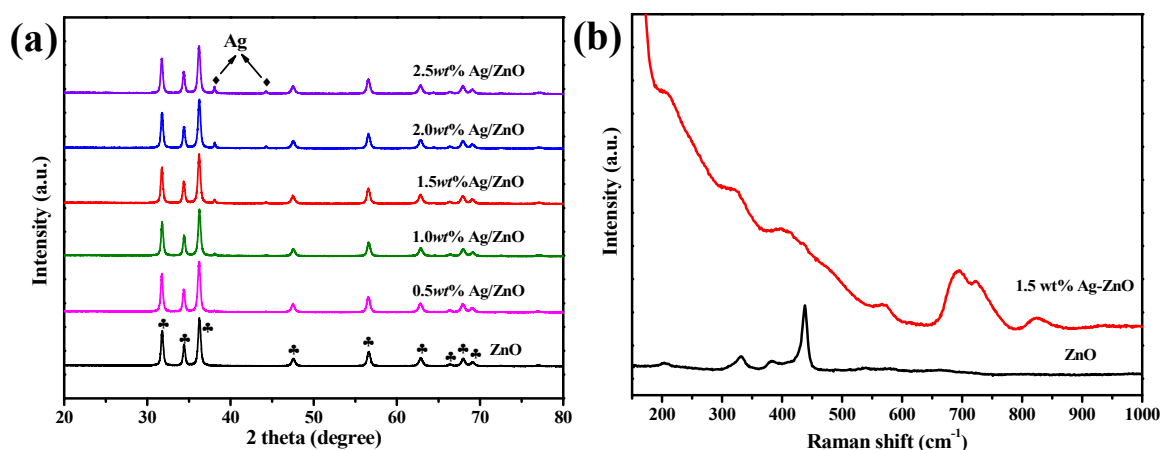


Figure 1. (a) XRD patterns and (b) Raman spectra of the samples.

SEM was taken to observe the morphology of pure ZnO and 1.5 wt% Ag/ZnO. In Figure 2, pure ZnO has a porous flake-like morphology composed of numerous aggregated nanoparticles and no obvious change in morphology is observed when ZnO is loaded with Ag. Ag/ZnO was further characterized by TEM. The porous structure is from the aggregation of ZnO nanoparticles (Figure 3a), which is in good agreement with the observation in the SEM image. The HR-TEM image (Figure 3b) clearly presents the lattice distance of 0.247 nm and 0.235 nm, corresponding to the (101) plane of

ZnO and the (111) plane of Ag [26], respectively. This means that the intimate contact between ZnO and Ag is formed, which will facilitate the separation for the photogenerated carriers of the catalyst. Meanwhile, the energy-dispersive X-ray spectroscopy (EDX) analysis was done to study the chemical constitution of Ag/ZnO. In Figure 3, Ag/ZnO comprises of three elements (O, Zn, and Ag) and the Ag element is well dispersed on the surface of ZnO. Additionally, the surface area and pore structure of ZnO and Ag/ZnO were studied by N<sub>2</sub>-sorption analysis (Figure S1). The surface area of Ag/ZnO (20 m<sup>2</sup>/g) is slightly lower than that of ZnO (25 m<sup>2</sup>/g). This could be attributed to the pore structure blocking by the Ag nanoparticles.

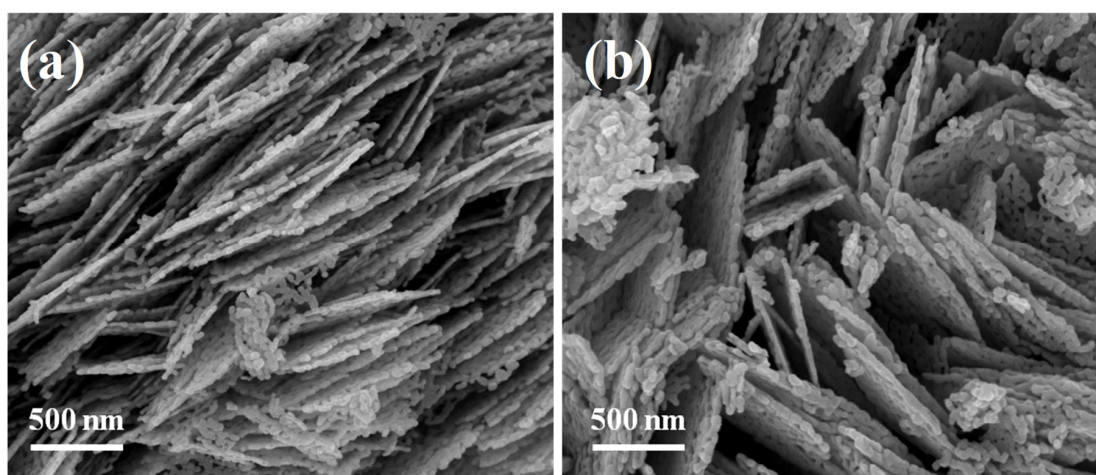


Figure 2. SEM images of (a) ZnO and (b) 1.5 wt% Ag/ZnO.

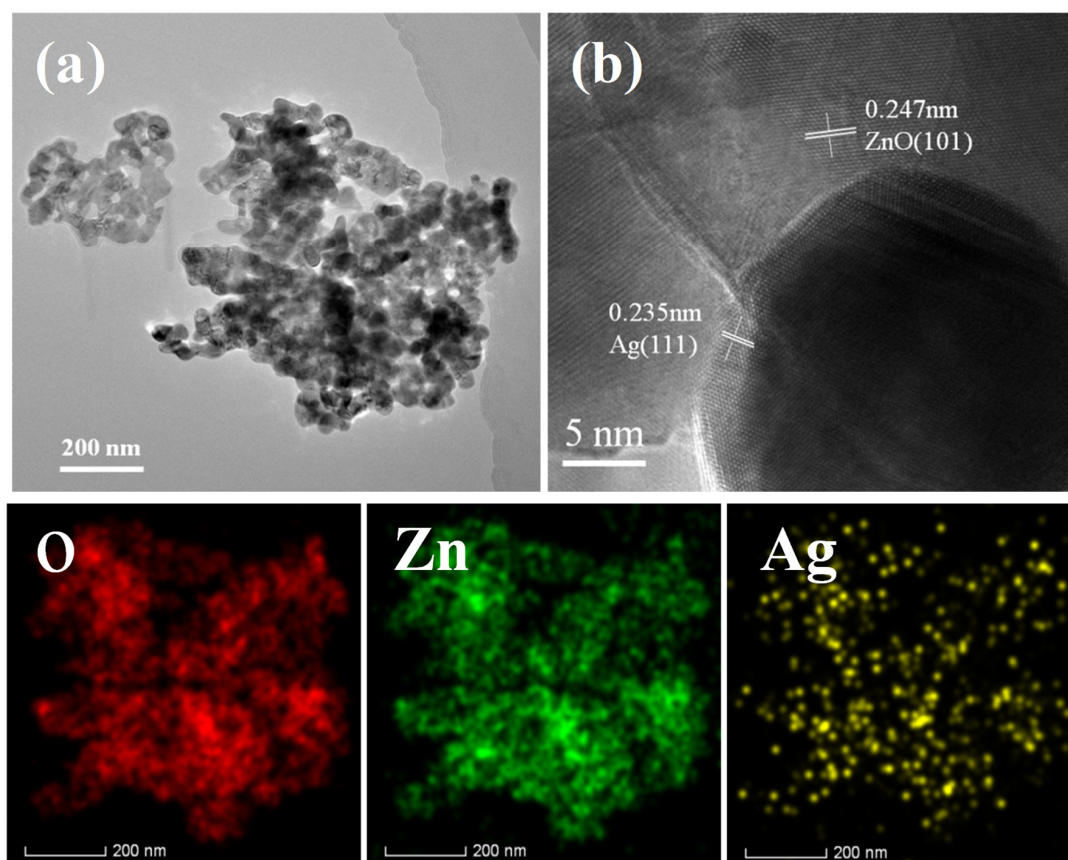
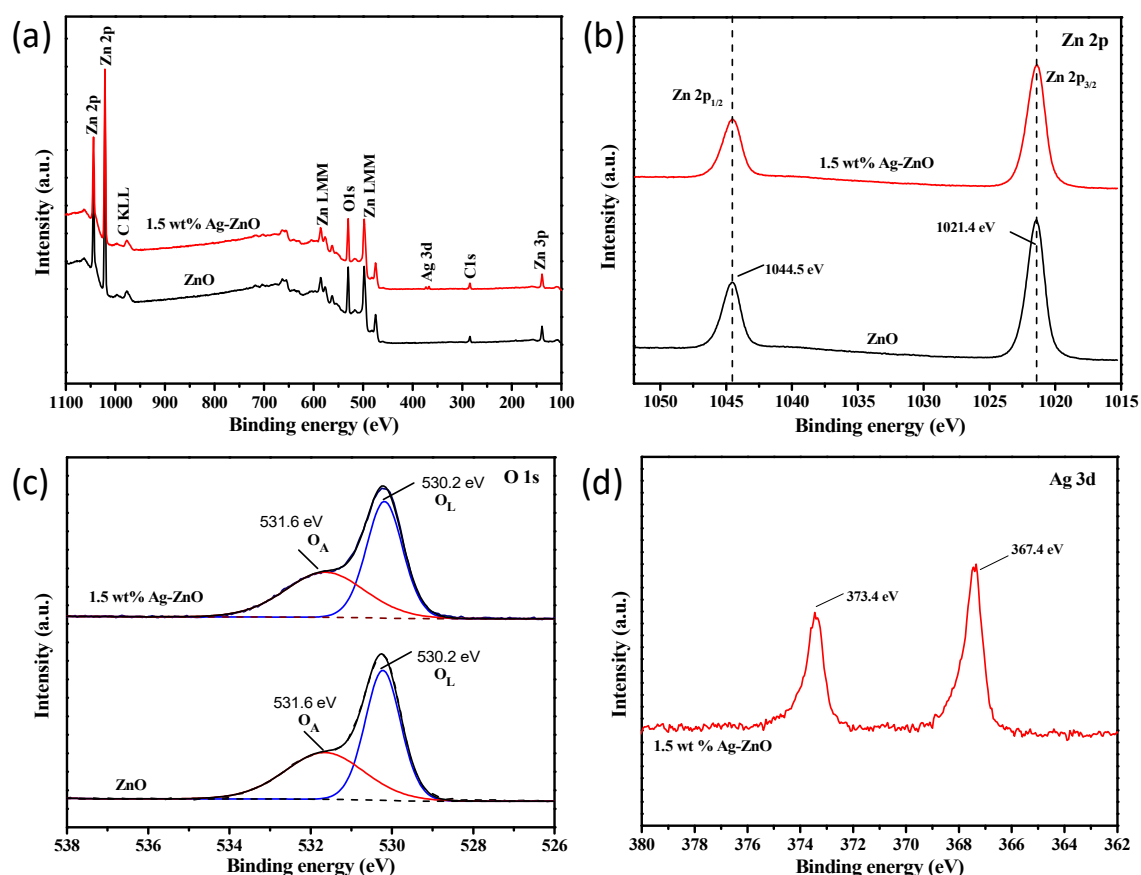


Figure 3. (a,b) TEM and energy-dispersive X-ray spectroscopy (EDX) mapping images of 1.5 wt% Ag/ZnO.

The chemical states of ZnO and Ag/ZnO were carefully examined by X-ray photoemission spectroscopy (XPS). In the survey spectra (Figure 4a), Zn, O, and C are present. ZnO, Zn, O, Ag, and C exist in the Ag/ZnO, and no other elements are observed. In Figure 4b, the Zn 2p spectra has two symmetrical peaks at 1021.4 and 1044.6 eV, corresponding to Zn 2p<sub>3/2</sub> and Zn 2p<sub>1/2</sub>, respectively. This is indicative of the presence of Zn<sup>2+</sup> in the samples, according to the reported data [30,31]. In Figure 4c, both samples present similar O1s spectra, which can be fitted into two peaks (531.7 eV and 530.2 eV), corresponding to the surface adsorbed oxygen and the lattice oxygen of ZnO [32], respectively. Figure 4d shows the Ag 3d XPS spectrum of Ag/ZnO. The two peaks centered at 373.4 and 367.4 eV correspond to Ag 3d<sub>3/2</sub> and Ag 3d<sub>5/2</sub>, respectively. The binding energies are much lower than those of pure metallic Ag (374.2 eV and 368.2 eV), indicative of the strong interaction and charge transfer between Ag and ZnO [33–35], which will favor the separation of the photogenerated charges and suppress their recombination.



**Figure 4.** The X-ray photoemission spectroscopy (XPS) spectra of ZnO and 1.5 wt% Ag/ZnO, (a) survey, (b) Zn 2p, (c) O 1s, and (d) Ag 3d.

Figure 5a displays the UV-Vis diffuse reflectance spectra of ZnO and Ag/ZnO. Pure ZnO has a strong absorption in the ultraviolet region (400 nm), in accordance with the wide band-gap feature of ZnO semiconductor. In comparison to ZnO, Ag/ZnO exhibits an extra absorption band in the visible region, which can be assigned to the strong surface plasmon resonance of the metallic Ag nanoparticle [36]. This also confirms that the as-synthesized sample is composed of metallic Ag and ZnO. Photoluminescence (PL) is a useful tool to get insightful evidence about the recombination of the photogenerated electron-hole pairs, thus the PL spectra for ZnO and Ag/ZnO were carried out. As shown in Figure 5b, there is a visible emission band around 600 nm in the PL spectra. The emission band may be due to the electron transition in various kinds of defect states [37]. It can be obviously seen that Ag/ZnO has a much lower emission intensity than bare ZnO, suggesting that the recombination of

photogenerated electron-hole couples is significantly suppressed [36]. This will facilitate the process involved in the participation of the photogenerated carriers in the reaction.

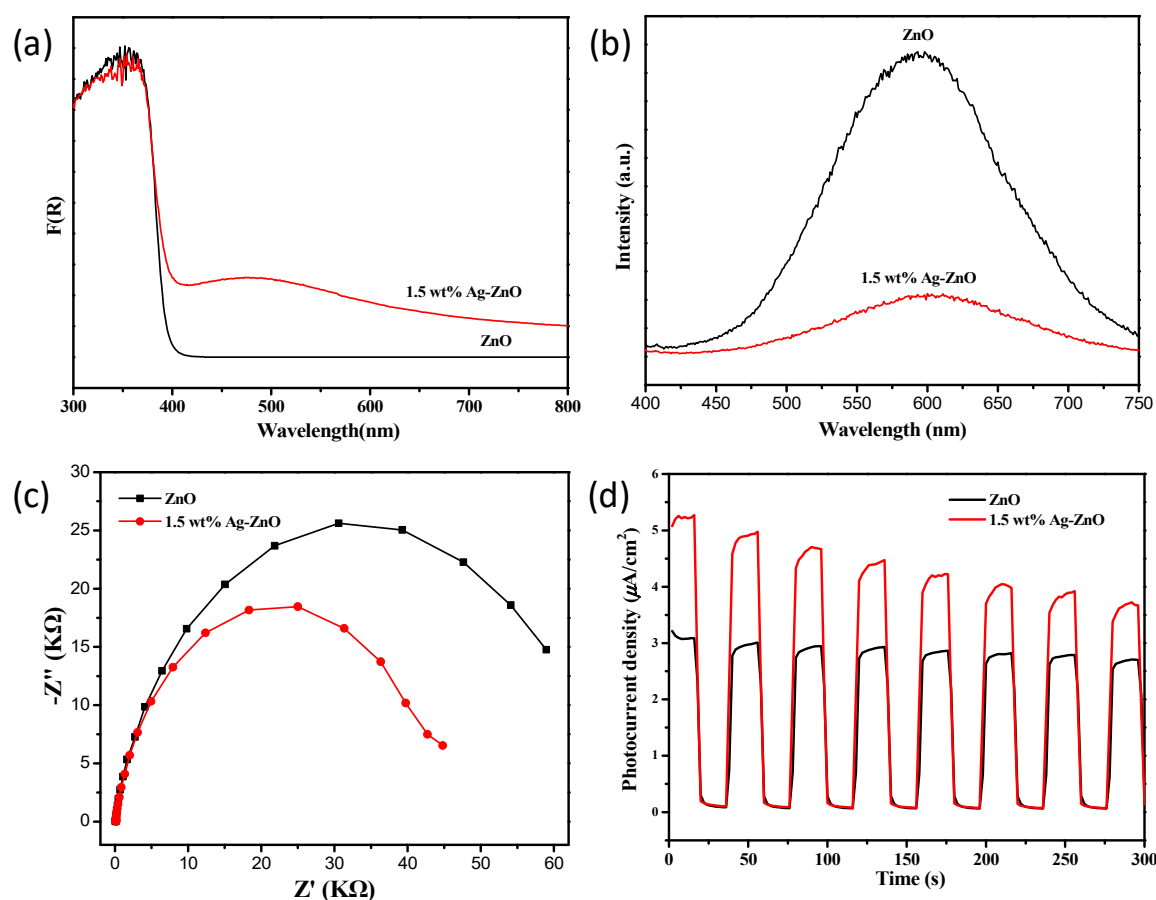


**Figure 5.** (a) The UV-Vis diffuse reflectance spectra, (b) the photoluminescence spectra, (c) electrochemical impedance spectroscopy (EIS) Nyquist plots, and (d) the photocurrent response curves of ZnO and 1.5 wt% Ag/ZnO.

Electrochemical impedance spectroscopy (EIS) has been commonly conducted to explore the charge transfer capability of the catalysts. The EIS Nyquist plots of ZnO and Ag/ZnO (Figure 5c) display semicircles related to the charge transfer resistance ( $R_{ct}$ ) across the catalyst-electrolyte interface. A smaller semicircle arc means a lower  $R_{ct}$  and faster charge transfer. Ag/ZnO shows a much smaller radius than bare ZnO, indicating that Ag deposition can promote the interfacial electron transfer [38]. The transient photocurrent response is closely associated with the separation efficiency of the photogenerated carriers. Generally, a higher photocurrent implies a higher separation efficiency of photogenerated electron-hole pairs. Figure 5d displays the photocurrent-time curves for ZnO and Ag/ZnO during repeated ON/OFF irradiation cycles. Ag/ZnO exhibits an enhanced photocurrent response compared to ZnO, suggesting that Ag/ZnO shows an enhanced efficiency in the photogenerated charges separation [39]. This will be advantageous to boost its activity in the photocatalytic ozonation reaction.

## 2.2. Activity

Phenol is a typical prevalent contaminant in wastewater streams and is often resistant to conventional water treatments. Thus, phenol was used as a model compound to evaluate the catalytic activities of ZnO and Ag/ZnO. Figure 6 shows the change of the normalized concentration of phenol and total organic carbon (TOC) as a function of the reaction time over different catalysts. The phenol and TOC removals are determined to 86% and 10% in the UV- $O_3$  process, respectively. When ZnO was

used as the catalyst in the UV-O<sub>3</sub> process, the phenol and TOC removals increased to 100% and 52%. Compared to pure ZnO, Ag/ZnO exhibited an enhanced performance and 1.5 wt% Ag/ZnO showed the best activity with the TOC removal of 62% in 60 min. Thus, we conducted the comprehensive comparison between 1.5 wt% Ag/ZnO and ZnO.

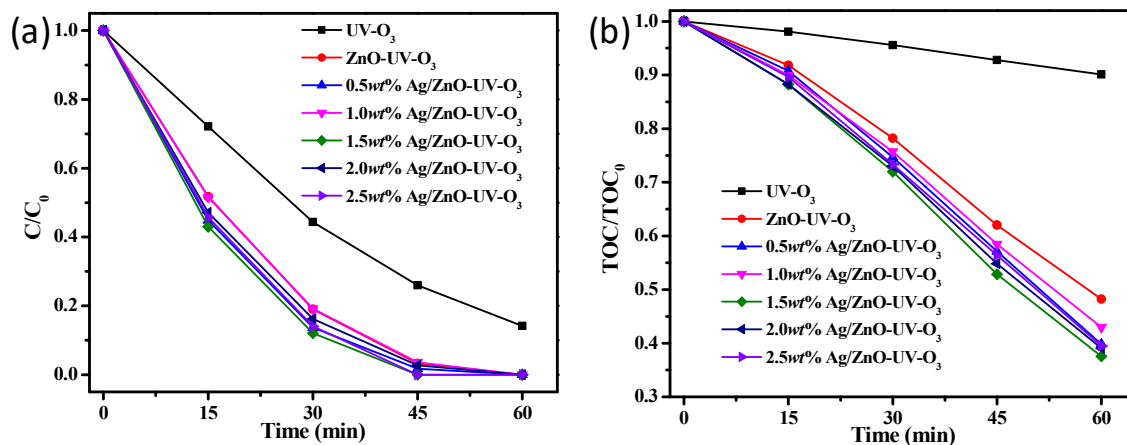


**Figure 6.** (a) The degradation and (b) mineralization of phenol in the photocatalytic ozonation process over ZnO and Ag/ZnO samples. Gaseous [O<sub>3</sub>]: 10 mg/L; O<sub>3</sub> flow rate: 50 mL/min; catalyst dosage: 0.5 g/L; phenol concentration: 50 mg/L.

To better understand the process of photocatalytic ozonation, we have studied the activities of ZnO and Ag/ZnO in different oxidation processes (Figure 7). There is no observable removal of phenol under UV irradiation in the absence of a catalyst. However, in the presence of ZnO, a rapid degradation of phenol occurs under UV irradiation. The introduction of ozone into the photocatalytic system can further increase the degradation rate of phenol (Figure 7a). The phenol degradation data can be expressed in a linear pattern using a pseudo-first kinetics model and the deduced kinetics constants are shown in Figure 7b. In the case of the ozonation process, ZnO behaves as a good catalyst for the phenol degradation efficiency and the corresponding kinetics constant is 0.05 min<sup>-1</sup>, about two times as high as that in ozone alone. The kinetics constant becomes slightly lower when ZnO is deposited with silver nanoparticles. It has been reported that Ag was an effective catalyst in decomposing ozone [40], thus the presence of silver nanoparticles might impair the utilization of ozone in the ozonation process. Interestingly, Ag/ZnO exhibits much higher photocatalytic activity than bare ZnO, which can be attributed to the higher photoinduced carrier separation by the formation of Ag/ZnO heterostructure. In the case of the combination of photocatalysis and ozonation, the kinetics constant of 0.07 min<sup>-1</sup> is achieved over Ag/ZnO, which is higher than that in the ZnO-UV-O<sub>3</sub> system (0.055 min<sup>-1</sup>). Furthermore, the kinetics constant is greatly larger than the sum of those in Ag/ZnO-UV (0.014 min<sup>-1</sup>) and O<sub>3</sub> (0.022 min<sup>-1</sup>). This enhancement in catalytic activity could be ascribed to the synergistic effects between photocatalysis and ozonation with Ag/ZnO. In addition, the Ag/Zn-UV-O<sub>3</sub> process exhibited better performance for phenol removal than the reported oxidation process with the ZnO-based catalyst (Table S1).

It is a vital issue whether or not the organic molecules can be completely oxidized into nontoxic CO<sub>2</sub> in oxidation reactions. Thus, the total of carbon (TOC) removal in different oxidation processes is also investigated in detail and the result is shown in Figure 7c,d. It exhibits a similar trend to the phenol removal in the different oxidation processes. In the system of Ag/ZnO-UV-O<sub>3</sub>, the TOC removal rate can reach 0.4 mg/L/min, which is higher than those in Ag/ZnO-UV (0.14 mg/L/min) and O<sub>3</sub> (0.03 mg/L/min). These results also illustrate the synergy which occurred in the photocatalytic ozonation process. Among the different processes, Ag/ZnO-UV-O<sub>3</sub> exhibits the best activity for the phenol degradation and mineralization. Additionally, the stability of Ag/ZnO in the photocatalytic ozonation of phenol was investigated. In Figure 8, the removal of phenol remained at nearly 100% and

the mineralization rate was kept at around 61% in the cyclic runs. Meanwhile, we also studied the  $\text{Ag}^+$  leaching in the photocatalytic ozonation process and the leaching amount of the Ag ion was 0.004, 0.006, 0.009, and 0.004 ppm in the four cycles, respectively. No obvious change is observed in the SEM image and the EDX analysis for Ag/ZnO after the reaction (Figure S2). This indicates that Ag/ZnO exhibits robust stability in the photocatalytic ozonation of phenol. Furthermore, this catalyst can be extensively used for the removal of tetracycline hydrochloride (Figure S3).

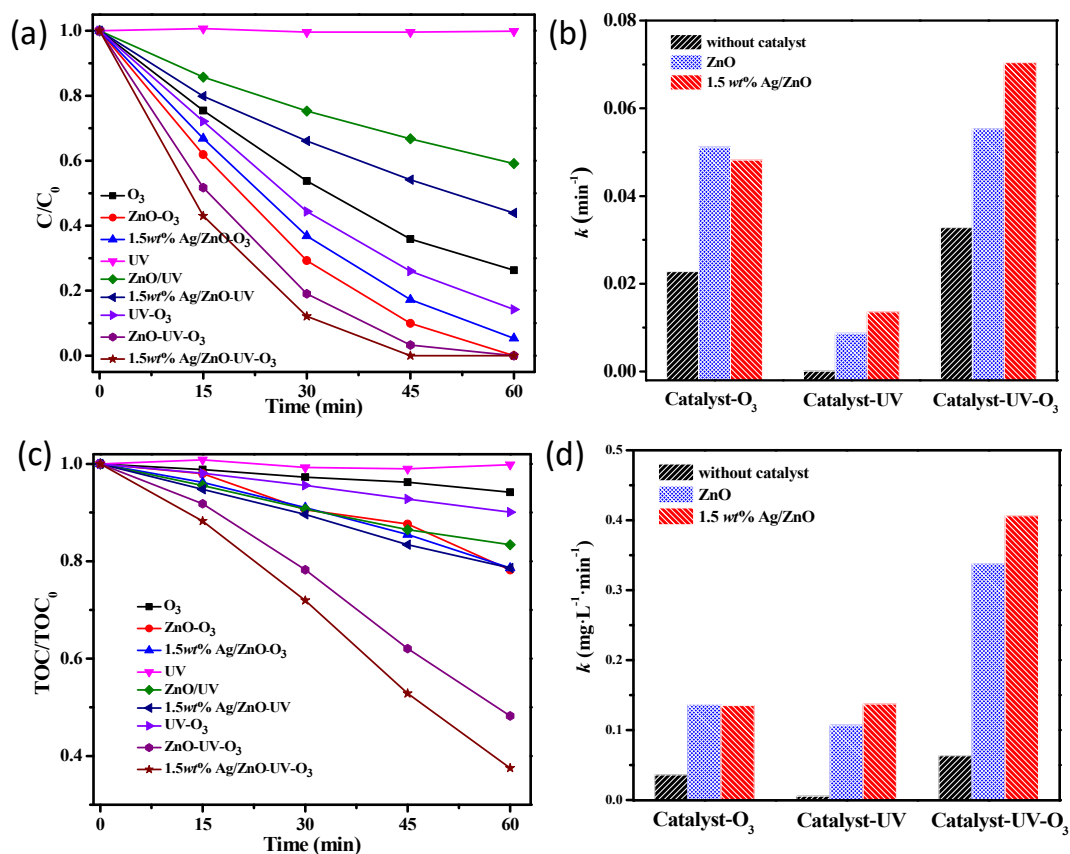


**Figure 7.** (a) The degradation and (c) mineralization of phenol in different oxidation processes, (b) the fitted kinetics degradation constants, and (d) TOC removal rates. Gaseous  $\text{O}_3$  concentration: 10 mg/L;  $\text{O}_3$  flow rate: 50 mL/min; catalyst dosage: 0.5 g/L; phenol concentration: 50 mg/L.

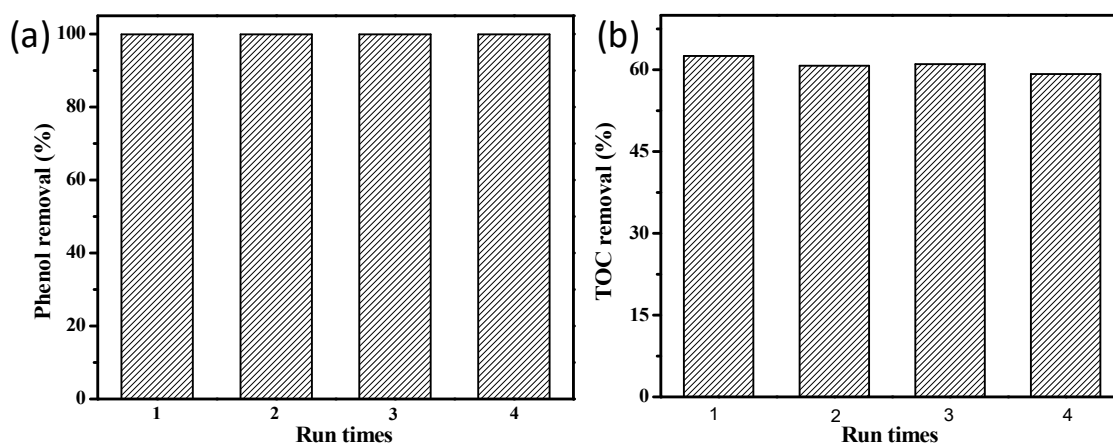


**Figure 8.** (a) The degradation and (b) mineralization of phenol in 60 min by a 1.5 wt% Ag/ZnO photocatalytic ozonation reaction for four cycles. Gaseous  $[\text{O}_3]$ : 10 mg/L;  $\text{O}_3$  flow rate: 50 mL/min; catalyst dosage: 0.5 g/L; phenol concentration: 50 mg/L.

### 2.3. Reaction Mechanism

To monitor the active species ( $\bullet\text{OH}$  and  $\bullet\text{O}_2^-$ ) generated in the photocatalytic ozonation process, EPR experiments were carried out.  $\bullet\text{OH}$  detection was done in the medium of ultrapure water. In Figure 9a, a four-line spectra with the intensity ratio of 1:2:2:1, characteristic of DMPO/ $\bullet\text{OH}$  [41,42], is observed over ZnO-UV- $\text{O}_3$  and Ag/ZnO-UV- $\text{O}_3$ , and no obvious DMPO/ $\bullet\text{OH}$  signal is found in the UV- $\text{O}_3$  process. It is well known that  $\bullet\text{OH}$  has strong oxidation ability and it can deeply mineralize the organic contaminants. Moreover, the  $\bullet\text{OH}$  produced in the Ag/ZnO-UV- $\text{O}_3$  system will result in a higher efficiency in the TOC removal. Methanol was used as the reaction medium instead of ultrapure water to detect  $\bullet\text{O}_2^-$ . Figure 9b clearly displays the EPR signals of the four-line spectra with the intensity ratio of 1:1:1:1, indicative of DMPO/ $\bullet\text{O}_2^-$  adducts [43–45]. When Ag/ZnO is employed as the catalyst, the intensity ratio is 1:1:1:1, indicative of DMPO/ $\bullet\text{O}_2^-$  adducts [43–45]. When Ag/ZnO is employed as the catalyst, the intensity of the DMPO/ $\bullet\text{O}_2^-$  signal is significantly increased. The produced active species also accelerate the removal and mineralization of phenol. To further verify the role of the active species in the phenol degradation over Ag/ZnO, the radical trapping experiments were carried out by using Tert-butanol (TBA) and p-benzoquinone (p-BQ) as the scavengers for  $\bullet\text{OH}$  and  $\bullet\text{O}_2^-$  [46,47], respectively. In Figure S4, the kinetics constants for phenol degradation dramatically decrease to  $0.03 \text{ min}^{-1}$  and  $0.005 \text{ min}^{-1}$  in the presence of 10 mM TBA and 10 mM p-BQ, respectively. This illustrates that both  $\bullet\text{OH}$  and  $\bullet\text{O}_2^-$  contribute to the decomposition of phenol, which is consistent with the EPR results.

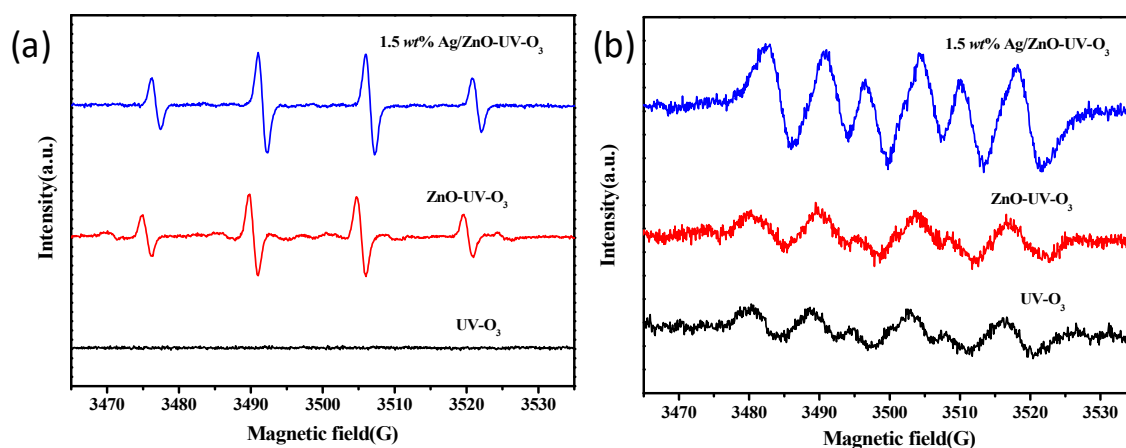


**Figure 9.** The electron paramagnetic resonance (EPR) spectra of DMPO/ $\bullet\text{OH}$  (a) and DMPO/ $\bullet\text{O}_2^-$  (b) over the UV- $\text{O}_3$  systems with different catalysts.

On the basis of the above results and analysis, the possible reaction mechanism for the photocatalytic ozonation of phenol over the Ag/ZnO catalyst was proposed. In Figure 10, when Ag/ZnO is irradiated with UV light, electrons are excited to the conduction band (CB) and holes are generated simultaneously in the valence band (VB). The photo-induced charges will migrate to the surface of ZnO, the holes oxidize phenol or react with  $\text{H}_2\text{O}$  to produce  $\bullet\text{OH}$ , and the photogenerated electrons in the conduction band of ZnO will quickly transfer to Ag nanoparticles by virtue of the intimate contact between ZnO and Ag. This will significantly reduce the recombination of the photogenerated electron-hole pairs. Meanwhile, the electrons will be trapped by  $\text{O}_3$  to produce active species such as  $\bullet\text{OH}$  and  $\bullet\text{O}_2^-$ , and these active species will efficiently degrade the organic pollutants and mineralize them into  $\text{CO}_2$ .

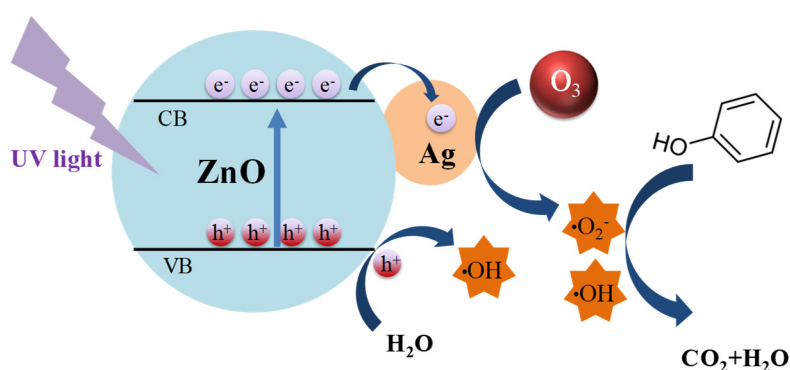


**Figure 10.** The proposed mechanism for the photocatalytic ozonation of phenol over Ag/ZnO.

### 3. Materials and Methods

#### 3.1. Catalyst Preparation and Characterization

Zn(CH<sub>3</sub>COO)<sub>2</sub>·2H<sub>2</sub>O (4.46 g) and CO(NH<sub>2</sub>)<sub>2</sub> (1.80 g) were dissolved in 40 mL deionized water, which was transferred into a 100 mL Teflon-lined stainless steel autoclave and then heated at 120 °C for 2 h. After the autoclave naturally cooled down to room temperature, the precipitation was filtered and washed with water/ethanol and then dried at 60 °C. ZnO was obtained by heating the dry precipitation at 400 °C for 2 h. Ag/ZnO was prepared by the photodeposition method. Typically, 0.60 g of ZnO powder was dispersed in 100 mL of the mixture of methanol and water (10%/90%, *v/v*) containing different amounts of AgNO<sub>3</sub> under stirring. The mixed suspension was irradiated with UV light for 30 min. The precipitate was then filtered, dried, and finally heated at 300 °C for 2 h. The sample was denoted as “*xwt%* Ag/ZnO”, where *x* is the theoretical value. The actual Ag loading amount was also determined by an inductively coupled plasma mass spectrometry (ICP) measurement (Table S2).

The crystal phase of the samples was identified by an X-ray Diffraction (XRD, Bruker D8 Advance, Germany) with Cu K $\alpha$  radiation ( $\lambda = 1.5406 \text{ \AA}$ ). The morphology and microstructure was characterized by scanning electron microscopy (SEM, Hitachi S4800, Japan) and transmission electron microscopy (TEM, FEI Talos F200S, Netherlands). Brunauer-Emmett-Teller specific surface area was determined on a Micromeritics ASAP2020 apparatus (USA). The UV-Vis diffuse reflectance spectra (DRS) of the samples were carried out on a Varian Cary 500 Scan. The X-ray photoelectron spectrum (XPS) was obtained by a PHI Quantum 2000 XPS (USA) with the C1s peak (284.6 eV) as a reference. The photoluminescence (PL) spectrum was measured on a Hitachi F900 fluorescence spectrophotometer (Japan). The electron spin resonance (ESR) spectrum was recorded using a Bruker model A300 spectrometer (Germany) to detect reactive species, with 5, 5-Dimethyl-1-pyrroline-N-oxide (DMPO) as the spin-trapping agent. The Ag leaching in the catalyst was investigated by inductively coupled plasma mass spectrometry (Avio 200, Perkin Elmer) in the photocatalytic ozonation process.

#### 3.2. Photocatalytic Ozonation Experiments

To evaluate catalytic activity of the catalysts, all experiments were conducted in the customized tubular quartz container (diameter: 50 mm; height: 250 mm) equipped with a sampling aperture, a long straight quartz tube ( $\phi 6 \times 1 \text{ mm}$ ) inserted into the bottom as ozone inlet. In a typical process for phenol removal, the tubular reactor contained a 160 mL suspension with 50 mg/L of phenol (pH = 6.8) and 0.5 g/L of the catalyst, surrounded by four portable UV lamps (Philips, BL 6W/10, 365 nm, Netherlands) and the gaseous ozone was continually bubbled into the reactor via the ozone inlet at a flow rate of 50 mL/min. During the run, a certain volume of the suspension was extracted from the reactor at each regular interval and then the supernate was obtained by using a 0.22  $\mu\text{m}$  microfilter for the phenol and the TOC analysis. The phenol concentration was determined by high performance liquid chromatography (HPLC) with a UV detector at 270 nm. The mixture of acetonitrile and water (30%/70%, *v/v*) was used as the mobile phase with a flow rate of 1.0 mL/min. The total organic carbon (TOC) of the

phenol solution was analyzed with a Shimadzu TOC-VCPH analyzer. Additionally, single ozonation, photocatalysis, and adsorption experiments were carried out as contrast experiments under similar conditions. To achieve the adsorption-desorption equilibrium of the phenol/catalyst, the suspension was stirred for 30 min in the dark before the reaction for all experiments.

#### 4. Conclusions

Ag/ZnO nanocomposites were successfully synthesized by a simple photodeposition approach and the catalysts were applied in the photocatalytic ozonation of organic wastewater. In comparison to bare ZnO, Ag/ZnO showed enhanced catalytic performance in the phenol removal and its mineralization, and the highest activity was achieved over 1.5 wt% Ag/ZnO. The synergy between photocatalysis and ozonation for phenol mineralization was also observed over Ag/ZnO, and it exhibited robust stability in the cyclic runs. Mechanism studies revealed, Ag loading promotes the separation and transfer efficiency of electron-holes on the surface of ZnO by virtue of the formed heterojunction between Ag and ZnO, thus more active species ( $\bullet\text{OH}$  and  $\bullet\text{O}_2^-$ ) are produced to drive the oxidation reaction for the advanced treatment of the organic pollutants. This investigation demonstrates an approach in developing efficient catalysts to advance photocatalytic ozonation for water decontamination.

**Supplementary Materials:** The following are available online at <http://www.mdpi.com/2073-4344/9/12/1006/s1>, Figure S1: The  $\text{N}_2$  adsorption-desorption isotherms for ZnO and 1.5 wt% Ag-ZnO, Figure S2: the SEM image and EDX analysis for 1.5 wt% Ag-ZnO after the reaction, Figure S3: The mineralization of tetracycline hydrochloride in different oxidation processes, Figure S4: The radical trapping experiments in the photocatalytic ozonation process using 1.5 wt% Ag/ZnO as a catalyst, Table S1: The recent reports on ZnO-based catalysts for phenol removal, Table S2: The ICP analysis of the Ag/ZnO samples.

**Author Contributions:** Conceptualization, Y.H.; investigation, J.P., T.L. and H.M.; writing—original draft preparation, J.P., Z.D., J.Z. and Y.H.; writing—review and editing, Z.Y. and Y.H.

**Funding:** This research was funded by National Key Technologies R&D Program of China (2014BAC13B03), NSFC (U1805255 and 21972022), Natural Science Foundation of Fujian Province (2018J01681), the Award Program for Outstanding Young Innovative Talents of Fujian province (00332111), and the Independent Research Project of State Key Laboratory of Photocatalysis on Energy and Environment (SKLPEE-2017A03).

**Conflicts of Interest:** The authors declare no conflict of interest.

#### References

1. Agustina, T.E.; Ang, H.M.; Vareek, V.K. A review of synergistic effect of photocatalysis and ozonation on wastewater treatment. *J. Photochem. Photobiol. C: Photochem. Rev.* **2015**, *6*, 264–273. [[CrossRef](#)]
2. Xiao, J.D.; Xie, Y.B.; Cao, H.B. Organic pollutants removal in wastewater by heterogeneous photocatalytic ozonation. *Chemosphere* **2015**, *121*, 1–17. [[CrossRef](#)] [[PubMed](#)]
3. Mehrjouei, M.; Muller, S.; Moller, D. A review on photocatalytic ozonation used for the treatment of water and wastewater. *Chem. Eng. J.* **2015**, *263*, 209–219. [[CrossRef](#)]
4. Pan, Z.H.; Cai, Q.H.; Luo, Q.; Li, X.W. Mechanism and kinetics of H-acid degradation in  $\text{TiO}_2/\text{O}_3/\text{UV}$  process. *Can. J. Chem. Eng.* **2014**, *92*, 851–860. [[CrossRef](#)]
5. Marque, G.; Rodriguez, E.M.; Maldonado, M.I.; Alvarez, P.M. Integration of ozone and solar  $\text{TiO}_2$ -photocatalytic oxidation for the degradation of selected pharmaceutical compounds in water and wastewater. *Sep. Purif. Technol.* **2014**, *136*, 18–26. [[CrossRef](#)]
6. Liu, X.L.; Guo, Z.; Zhou, L.B.; Yang, J.; Cao, H.B.; Xiong, M.; Xie, Y.B.; Jia, G.R. Hierarchical biomimetic  $\text{BiVO}_4$  for the treatment of pharmaceutical wastewater in visible-light photocatalytic ozonation. *Chemosphere* **2019**, *222*, 38–45. [[CrossRef](#)] [[PubMed](#)]
7. Yang, J.; Xiao, J.D.; Cao, H.B.; Guo, Z.; Rabeah, J.; Bruckner, A.; Xie, Y.B. The role of ozone and influence of band structure in  $\text{WO}_3$  photocatalysis and ozone integrated process for pharmaceutical wastewater treatment. *J. Hazard. Mater.* **2018**, *360*, 481–489. [[CrossRef](#)]
8. Rey, A.; Mena, E.; Chavez, A.M.; Beltran, F.J.; Medina, F. Photocatalytic water treatment over  $\text{WO}_3$  under visible light irradiation combined with ozonation. *Chem. Phys. Lett.* **2010**, *500*, 86–89.

9. Mano, T.; Nishimoto, S.; Kameshima, Y.; Miyake, M. Water treatment efficacy of various metal oxide semiconductors for photocatalytic ozonation under UV and visible light irradiation. *Chem. Eng. J.* **2015**, *264*, 221–229. [[CrossRef](#)]
10. Ling, Y.; Liao, G.Z.; Xu, P.; Li, L.S. Fast mineralization of acetaminophen by highly dispersed Ag/g-C<sub>3</sub>N<sub>4</sub> hybrid assisted photocatalytic ozonation. *Sep. Purif. Technol.* **2019**, *216*, 1–8. [[CrossRef](#)]
11. Yin, J.; Liao, G.Z.; Zhou, J.L.; Huang, C.M.; Ling, Y.; Lu, P.; Li, L.S. High performance of magnetic BiFeO<sub>3</sub> nanoparticle-mediated photocatalytic ozonation for wastewater decontamination. *Sep. Purif. Technol.* **2016**, *168*, 134–140. [[CrossRef](#)]
12. Lee, K.M.; Lai, C.W.; Ngai, K.S.; Juan, J.C. Recent developments of zinc oxide based photocatalyst in water treatment technology: A review. *Water Res.* **2016**, *88*, 428–448. [[CrossRef](#)] [[PubMed](#)]
13. Orge, C.A.; Soares, O.; Ramalho, P.S.F.; Pereira, M.F.R.; Faria, J.L.; Salomé, G.P. Magnetic nanoparticles for photocatalytic ozonation of organic pollutants. *Catalysts* **2019**, *9*, 703. [[CrossRef](#)]
14. Zhai, X.; Chen, Z.L.; Zhao, S.Q.; He, W.; Yang, L. Enhanced ozonation of dichloroacetic acid in aqueous solution using nanometer ZnO powders. *J. Environ. Sci.* **2010**, *22*, 1527–1533. [[CrossRef](#)]
15. Yuan, X.J.; Yan, X.; Xu, H.M.; Li, D.Y.; Sun, L.; Cao, G.; Xia, D.S. Enhanced ozonation degradation of atrazine in the presence of nano-ZnO: Performance, kinetics and effects. *J. Environ. Sci.* **2017**, *61*, 3–13. [[CrossRef](#)] [[PubMed](#)]
16. Wu, J.F.; Su, T.M.; Jiang, Y.X.; Xie, X.L.; Qin, Z.Z.; Ji, H.B. In situ DRIFTS study of O<sub>3</sub> adsorption on CaO, gamma-Al<sub>2</sub>O<sub>3</sub>, CuO, alpha-Fe<sub>2</sub>O<sub>3</sub> and ZnO at room temperature for the catalytic ozonation of cinnamaldehyde. *Appl. Surf. Sci.* **2019**, *412*, 290–305. [[CrossRef](#)]
17. Chen, W.H.; Liu, Q.F.; Tian, S.Q.; Zhao, X.J. Exposed facet dependent stability of ZnO micro/nano crystals as a photocatalyst. *Appl. Surf. Sci.* **2019**, *470*, 807–816. [[CrossRef](#)]
18. Lam, S.M.; Sin, J.C.; Abdullah, A.Z.; Mohamed, A.R. Degradation of wastewaters containing organic dyes photocatalysed by zinc oxide: A review. *Desalin. Water Treat.* **2012**, *41*, 131–169. [[CrossRef](#)]
19. Jing, L.Q.; Zhou, W.; Tian, G.H.; Fu, H.G. Surface tuning for oxide-based nanomaterials as efficient photocatalysts. *Chem. Soc. Rev.* **2013**, *42*, 9509–9549. [[CrossRef](#)]
20. Jing, L.Q.; Wang, D.J.; Wang, B.Q.; Li, S.D.; Xin, B.F.; Fu, H.G.; Sun, J.Z. Effects of noble metal modification on surface oxygen composition, charge separation and photocatalytic activity of ZnO nanoparticles. *J. Mol. Catal. A: Chem.* **2006**, *244*, 193–200.
21. Qi, K.Z.; Cheng, B.; Yu, J.G.; Ho, W.K. Review on the improvement of the photocatalytic and antibacterial activities of ZnO. *J. Alloys Compd.* **2017**, *727*, 792–820. [[CrossRef](#)]
22. Liu, X.Q.; Iocozzia, J.; Wang, Y.; Cui, X.; Chen, Y.H.; Zhao, S.Q.; Li, Z.; Lin, Z.Q. Noble metal-metal oxide nanohybrids with tailored nanostructures for efficient solar energy conversion, photocatalysis and environmental remediation. *Energy Environ. Sci.* **2017**, *10*, 402–434. [[CrossRef](#)]
23. Wu, A.P.; Tian, C.G.; Yan, H.J.; Hong, Y.; Jiang, B.J.; Fu, H.G. Intermittent microwave heating-promoted rapid fabrication of sheet-like Ag assemblies and small-sized Ag particles and their use as co-catalyst of ZnO for enhanced photocatalysis. *J. Mater. Chem. A* **2014**, *2*, 3015–3023. [[CrossRef](#)]
24. Xie, W.; Li, Y.Z.; Sun, W.; Huang, J.C.; Xie, H.; Zhao, X.J. Surface modification of ZnO with Ag improves its photocatalytic efficiency and photostability. *J. Photochem. Photobiol. A* **2010**, *216*, 149–155. [[CrossRef](#)]
25. Raji, R.; Sibi, K.S.; Gopchandran, K.G. ZnO: Ag nanorods as efficient photocatalysts: Sunlight driven photocatalytic degradation of sulforhodamine B. *Appl. Surf. Sci.* **2019**, *427*, 863–875.
26. Zhua, X.L.; Liang, X.H.; Wang, P.; Dai, Y.; Huang, B.B. Porous Ag-ZnO microspheres as efficient photocatalyst for methane and ethylene oxidation: Insight into the role of Ag particles. *Appl. Surf. Sci.* **2018**, *456*, 493–500. [[CrossRef](#)]
27. Wang, R.P.; Xu, G.; Jin, P. Size dependence of electron-phonon coupling in ZnO nanowires. *Phys. Rev. B* **2004**, *69*, 13303–13304. [[CrossRef](#)]
28. Zhu, G.; Liu, Y.; Xu, H.; Chen, Y.; Shen, X.; Xu, Z. Photochemical deposition of Ag nanocrystals on hierarchical ZnO microspheres and their enhanced gas-sensing properties. *CrystEngComm* **2012**, *14*, 719–725. [[CrossRef](#)]
29. Cacciato, G.; Bayle, M.; Pugliara, A.; Bonafos, C.; Zimbone, M.; Privitera, V.; Grimaldi, M.G.; Carles, R. Enhancing carrier generation in TiO<sub>2</sub> by a synergistic effect between plasmon resonance in Ag nanoparticles and optical interference. *Nanoscale* **2015**, *7*, 13468–13476. [[CrossRef](#)]

30. Mou, H.; Song, C.; Zhou, Y.; Zhang, B.; Wang, D. Design and synthesis of porous Ag/ZnO nanosheets assemblies as super photocatalysts for enhanced visible-light degradation of 4-nitrophenol and hydrogen evolution. *Appl. Catal. B Environ.* **2018**, *221*, 565–573. [CrossRef]
31. Liu, Y.T.; Zhanga, Q.P.; Xua, M.; Yuan, H.; Chen, Y.; Zhang, J.; Luo, K.; Zhang, J.Q.; You, B. Novel and efficient synthesis of Ag-ZnO nanoparticles for the sunlight induced photocatalytic degradation. *Appl. Surf. Sci.* **2019**, *476*, 632–640. [CrossRef]
32. Zheng, Y.H.; Zheng, L.R.; Zhan, Y.Y.; Lin, X.Y.; Zheng, Q.; Wei, K.M. Ag/ZnO heterostructure nanocrystals: Synthesis, characterization, and photocatalysis. *Inorg. Chem.* **2007**, *46*, 6980–6986. [CrossRef] [PubMed]
33. Lu, W.; Gao, S.; Wang, J. One-pot synthesis of Ag/ZnO self-assembled 3D hollow microspheres with enhanced photocatalytic performance. *J. Phys. Chem. C* **2008**, *112*, 16792–16800. [CrossRef]
34. Liu, X.; Li, W.; Chen, N.; Xing, X.X.; Dong, C.J.; Wang, Y.D. Ag-ZnO heterostructure nanoparticles with plasmon-enhanced catalytic degradation for Congo red under visible light. *RSC Adv.* **2015**, *5*, 34456–34465. [CrossRef]
35. Lai, Y.; Meng, M.; Yu, Y. One-step synthesis, characterizations and mechanistic study of nanosheets-constructed fluffy ZnO and Ag/ZnO spheres used for Rhodamine B photodegradation. *Appl. Catal. B: Environ.* **2010**, *100*, 491–501. [CrossRef]
36. Vaiano, V.; Matarangolo, M.; Murcia, J.J.; Rojas, H.; Navío, J.A.; Hidalgo, M.C. Enhanced photocatalytic removal of phenol from aqueous solutions using ZnO modified with Ag. *Appl. Catal. B: Environ.* **2018**, *225*, 197–206. [CrossRef]
37. Hasabeldaim, E.H.H.; Ntwaeaborwa, O.M.; Kroon, R.E.; Coetsee, E.; Swart, H.C. Enhanced green luminescence from ZnO nanorods. *J. Vac. Sci. Technol. B* **2019**, *37*, 011201. [CrossRef]
38. Nouri, H.; Habibi-Yangjeh, A.; Azadi, M. Preparation of Ag/ZnMgO nanocomposites as novel highly efficient photocatalysts by one-pot method under microwave irradiation. *J. Photochem. Photobiol. A* **2014**, *281*, 59–67. [CrossRef]
39. Huang, M.L.; Weng, S.X.; Wang, B.; Hu, J.; Fu, X.Z.; Liu, P. Various facet tunable ZnO crystals by a scalable solvothermal synthesis and their facet-dependent photocatalytic activities. *J. Phys. Chem. C* **2014**, *18*, 25434–25440. [CrossRef]
40. Imamur, S.; Ikebata, M.; Ito, T.; Ogita, T. Decomposition of ozone on a silver catalyst. *Ind. Eng. Chem. Res.* **1991**, *30*, 217–221. [CrossRef]
41. Wang, X.Y.; Wang, A.Q.; Ma, J. Visible-light-driven photocatalytic removal of antibiotics by newly designed C<sub>3</sub>N<sub>4</sub>@MnFe<sub>2</sub>O<sub>4</sub>-graphene nanocomposites. *J. Hazard. Mater.* **2017**, *336*, 81–92. [CrossRef] [PubMed]
42. Ding, J.; Dai, Z.; Qin, F.; Zhao, H.P.; Zhao, S.; Chen, R. Z-scheme BiO<sub>1-x</sub>Br/Bi<sub>2</sub>O<sub>2</sub>CO<sub>3</sub> photocatalyst with rich oxygen vacancy as electron mediator for highly efficient degradation of antibiotics. *Appl. Catal. B: Environ.* **2017**, *205*, 281–291. [CrossRef]
43. Zheng, Y.; Yu, Z.H.; Lin, F.; Guo, F.S.; Alamry, K.A.; Taib, L.A.; Asiri, A.M.; Wang, X.C. Sulfur-doped carbon nitride polymers for photocatalytic degradation of organic pollutant and reduction of Cr(VI). *Molecules* **2017**, *22*, 572. [CrossRef] [PubMed]
44. Yu, L.H.; Zhang, X.Y.; Li, G.W.; Cao, Y.T.; Shao, Y.; Li, D.Z. Highly efficient Bi<sub>2</sub>O<sub>2</sub>CO<sub>3</sub>/BiOCl photocatalyst based on heterojunction with enhanced dye-sensitization under visible light. *Appl. Catal. B: Environ.* **2016**, *187*, 301–309. [CrossRef]
45. Dong, Y.M.; Yang, H.X.; He, K.; Wu, X.; Zhang, A.M. Catalytic activity and stability of Y zeolite for phenol degradation in the presence of ozone. *Appl. Catal. B: Environ.* **2008**, *82*, 163–168. [CrossRef]
46. Yang, T.T.; Peng, J.M.; Zheng, Y.; He, X.; Hou, Y.; Wu, L.; Fu, X. Enhanced photocatalytic ozonation degradation of organic pollutants by ZnO modified TiO<sub>2</sub> nanocomposites. *Appl. Catal. B: Environ.* **2018**, *221*, 223–234. [CrossRef]
47. Li, W.J.; Li, D.Z.; Lin, Y.M.; Wang, P.X.; Chen, W.; Fu, X.Z.; Shao, Y. Evidence for the active species involved in the photodegradation process of methyl orange on TiO<sub>2</sub>. *J. Phys. Chem. C* **2012**, *116*, 3552–3560. [CrossRef]

